

Methodology for the In-situ Observation of Alporas Foams Using X-ray Radioscopy

K. Kadoi

*Graduate School of Sci. and Eng., Waseda Univ.
2-8-26, Nishiwaseda, Shinjuku
1690051 Tokyo, Japan*

H. Nakae

*Research Institute for Materials Sci. and Tech.
Waseda University
2-8-26, Nishiwaseda, Shinjuku
1690051 Tokyo, Japan*

J. Banhart

*Department of Materials Science (SF3)
Hahn-Meitner-Institut Berlin GmbH
Glienicke Straße 100
14109 Berlin, Germany*

N. Babcsán

*Bay Zoltán Foundation for Applied Research
Fehérvári út 130.
1116 Budapest, Hungary*

F. García-Moreno

*Department of Materials Science (SF3)
Hahn-Meitner-Institut Berlin GmbH
Glienicke Straße 100
14109 Berlin, Germany*

ABSTRACT

We carried out in-situ X-ray radioscopy experiments on Alporas-type foams during foaming using a microfocus X-ray imaging system. The foams were produced in the X-ray chamber by reheating precursors prepared previously by melting pure aluminium, adding 1.5 wt.% Ca, stirring for 20 minutes, adding 1.5 wt.% TiH₂, stirring again for 20 to 100 s and finally quenching the liquid mixture by inserting a cold steel lance into the melt from the top. Foaming of such precursors upon reheating was analyzed using the X-ray image sequences which were continuously acquired and by applying an image analysis program. Due to the fast decomposition of TiH₂ already during manufacture of the precursor a certain level of porosity was found even when applying short mixing times. The influence of such precursor porosity on foam expansion is notable. The quality of the blowing agent significantly influenced foam evolution.

INTRODUCTION

Some of the most prominent properties of closed cell aluminium foams are their low density, high specific strength, high energy absorption, etc. [1, 2]. Due to these advantages, aluminium foams are very attractive materials for e.g. automobile and aerospace applications, where

weight reduction and improvement in safety are requested. The performance of the foams is affected mainly by their density, cell size and wall thickness. The final structure is influenced by the stability of liquid metal and the processing parameters [2, 3, 4, 5, 6].

Several metal foam production methods have been proposed and are now being applied by the industry [1,2]. Foam evolution - which includes foam formation, liquid drainage and solidification - depends on the way the gas is supplied into the melt and the stability of liquid structural elements of the foams [7]. The gas supply can be external (gas injection) or internal (blowing agent). In the external case, the gas is injected by using an injector which is set at the bottom of the melt [2,6]. Alternatively, TiH₂ powder which usually is used as the blowing agent is added to the melt which is then stirred vigorously [2,3]. Currently, some foams are exploited commercially under trade names such as “Cymat” (external) [8], “Metcomb” (external) [9] and “Alporas” (internal) [3,10]. The latter is at present one of the commercially most successful aluminium-based foams.

Alporas [3,10,11] foam is manufactured by a batch casting process, which consists of several steps, namely thickening, foaming, cooling and cutting. The standard composition of Alporas is Al1.6Ca + 1.5 wt.% Ti. Calcium acts as a thickening agent. After admixing it to the melt and stirring for 6 min in ambient atmosphere stabilizing particles are formed by oxidation [3]. In the foaming stage 1.5 wt.%

TiH₂ powder is added to the thickened melt which is stirred again. Up to now, several investigations were carried out about the Alporas process. These reports reveal that foamability can be controlled by the processing parameters, namely stirring conditions and holding time in a furnace [3, 12]. In addition, the viscosity is one of the factors which is influencing the stability [3,13,14]. Despite this discussion about foam evolution, the stabilization mechanism of such foams is still subject of some debate.

For the investigation of foam stability, both in-situ (in the liquid state) and ex-situ (after solidification) analyses can be applied. The former method reveals in real time the architectural changes during foam evolution, the latter reveals the details of microstructure. In our previous publication in-situ analyses were carried out to survey foam stability using X-rays [6,15]. Garcia-Moreno et al. studied drainage phenomena during foaming of compacted powder precursors in-situ [15]. Babcsán et al. investigated the foaming of melts by external gas blowing with the same technique [6]. The aim of this work is to establish this experimental technique for the study the Alporas-type foams and to study their evolution in real time.

EXPERIMENTAL

The experimental procedure was divided into three processing stages, *thickening*, *mixing* and *foaming*, according to the Alporas process. To simplify experiments and analyses, pure aluminium as matrix material, calcium as thickening agent and TiH₂ powder as blowing agent were used.

(1) Thickening

In the first step, thickened samples were fabricated. 700 g of pure aluminium was melted and held at 700°C. 1.5 wt.% calcium was added to the melt as a thickening agent and stirred for 20 min by using a double propellers system [14]. The stirring system consisted of an electrical furnace, a motor and a torque meter. The crucible (top diameter 100 mm, bottom diameter 60 mm, height 100 mm) and the propeller were made of steel and coated with Al₂O₃ suspension to prevent the reaction with the aluminium melt. In order to monitor the course of the stirring torque, the value was measured during stirring once per second by a torque meter. After thickening the sample was poured into an insulating sleeve and cooled on a copper plate in air.

(2) Mixing

50 g of the prepared material was cut and melted at 700 °C. In the next step, 1.5 wt.% TiH₂ was admixed. In this stage the stirring device was similar to that used in the *thickening* stage. A smaller stainless steel crucible (top diameter 77 mm, bottom diameter 50 mm, height 96 mm) and a single propeller were used due to the reduced amount of material involved compared to the thickening stage (with $H=5$ mm propeller height, $\theta=45^\circ$ propeller angle applying 900 rpm of the stirrer). TiH₂ powder was supplied by Toho Titanium Co. LTD., Japan (purity 98.9 %, nominal grain size < 45 µm). Prior to addition to the melt the TiH₂ powders

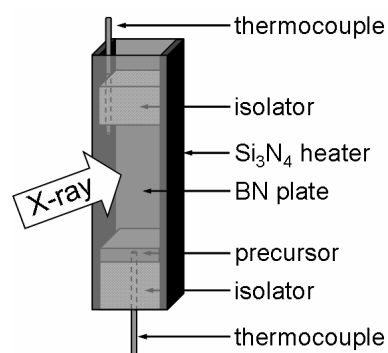


Figure. 1 Schematic illustration of the X-ray transparent foaming furnace.

were dehumidified at 150°C for 24 h and then wrapped in an aluminium foil and added to the melt in order to achieve a good yield. The foam samples were fabricated by mixing for 20, 50 and 100 s. The stirring speed of the mixing and the applied mixing times were optimized using literature data [12]. After mixing the melt was quenched by inserting a cold steel lance into the melt from the top which led to quick solidification. 4×10×10 mm³ samples for the *foaming* experiments were cut from that part of the quenched sample which was directly in contact with the steel lance.

(3) Foaming

The samples were heated to above the liquidus temperature and were kept there at 700 °C during the experiment, 500 s, by using a Si₃N₄-encased heater as shown in Fig. 1. The heater was controlled by a PID controller linked to the furnace thermocouple during the entire thermal cycle. For the in-situ radiosopic investigation, foam evolution was monitored by the X-ray imaging device, a 150 kV microfocus X-ray source from Hamamatsu, Japan) with 5 to 50 µm spot size and a detector also from Hamamatsu used in the 4×4-binning mode of the array of 560×592 pixels (vertical×horizontal) panel detector as described previously [16]. Radioscopic images were taken every 2 s during foam expansion and decay. The sample and furnace temperatures were measured by K-type thermocouples. Foam expansion was carried out directionally by enclosing the volume with boron nitride plates and Si₃N₄ heaters. A program named “AXIM” was used for the image analysis of drainage [16]. For this analysis an area in which the thermocouple was not visible was chosen. Vertical density profiles were calculated from the integrated grey level of horizontal pixel lines. This grey level corresponds to attenuated X-ray intensity I following the relation:

$$I = I_0 e^{-\mu d} \quad (1)$$

Where μ is the linear attenuation coefficient and d the total thickness of the liquid metal transversed by the beam, which in turn is proportional to the local foam density.

RESULTS and DISCUSSION

Fig. 2 gives three X-ray images of TiH_2 filled precursors and the corresponding foams in their maximum expansion stages for different mixing times. The porosities of the precursors were 52.8% after 20 s, 38.0% after 50 s and 33.3% after 100 s. It can be seen also in Fig. 2 that each of the precursors contained a considerable level of porosity which was formed by the fast release of hydrogen immediately after admixture of TiH_2 . As the flux of hydrogen release decreases with time [17] the growing rate of the pores also decreases. Thus, the size and the amount of pores become smaller with increasing mixing time. Besides porosity changes in the precursor, the influence of mixing time on maximum expansion is also significant (Fig. 2). As the amount of TiH_2 was equal, shorter mixing times should lead to higher expansion of the foam due to less hydrogen losses during precursor production. However, the measured maximum expansion in Fig. 2 indicates the opposite effect. A larger expansion after longer mixing time could be explained if we assume more pore nucleation by longer stirring time and an equal growing rate of bubbles. In this way it was found that the early pore density is an important factor for further foam evolution. 100 s of stirring time of the precursor has been chosen for our further studies.

A typical temperature profile of the furnace and the precursor is shown in Fig. 3. The heating phase of the furnace starts after 10 s and continues during the following approximately 70 s. After this point, the temperature is kept constant at 700 °C. The sample temperature falls behind the furnace temperature in the initial heating stage due to the thermal inertia of the system. Furthermore, in case of sample's profile, there is an inflection point at 625 °C which represents the melting temperature of the matrix as verified by a differential scanning calorimetry (DSC) measurement.

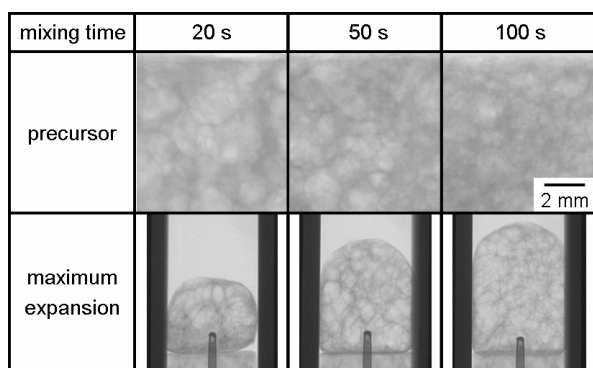


Figure 2. X-ray radioscopic images of precursors and corresponding foams at maximum expansion for three different mixing times.

Fig. 4 shows various images reflecting foam evolution corresponding to the heating profile given in Fig. 3. The sample begins to foam after 70 s at the sides where the temperature is locally higher and has already melted. After the temperature has reached the liquidus temperature at $t=80$ s, the growing rate is much faster than in the solid state. The

foam reaches maximum expansion within 20 s (at $t=100$ s). After maximum expansion, decay and drainage occur and bubbles grow due to coalescence. After significant collapse, shrinkage starts in the lower part of the sample although the foam is still in the liquid state and the temperature is kept constant. Decay continues for more than 300 s, and a remarkable shrinkage most likely due to hydrogen effusion and loss causes the final collapse of the foam (Fig. 4h). From the literature it is known that decomposition of TiH_2

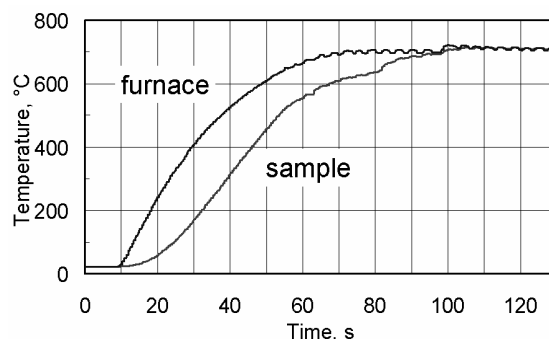


Figure 3. Temperature profiles of the sample and the furnace.

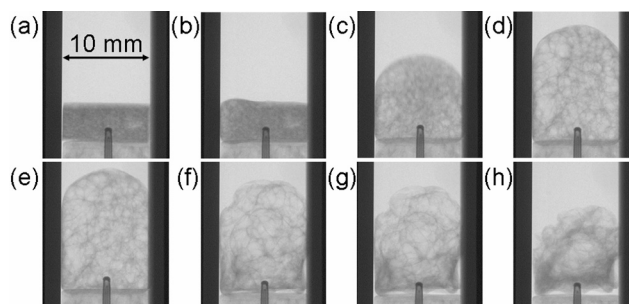


Figure 4. Typical foam evolution. Images show states, (a) 0 s, (b) 70 s, (c) 80 s, (d) 90 s, (e) 100 s, (f) 150 s, (g) 200 s and (h) 400 s.

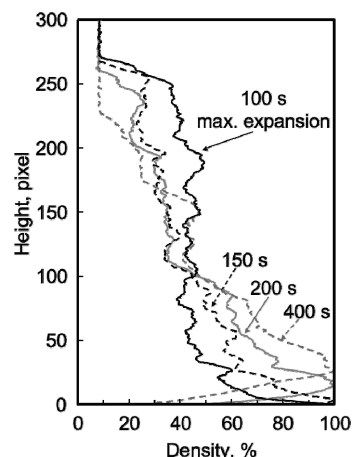


Figure 5. Typical density profile of a foam.

starts at around 380 °C and continues for more than 10 min [11,17]. Thus, we can assume that foam collapse is caused by hydrogen escape from the foam which has been degraded by drainage and coalescence.

Density distribution curves before and after maximum expansion are given in Fig. 5. They indicate that the liquid is uniformly dispersed in the sample near the maximum expansion stage. After maximum expansion, however, density decreases at the upper part of foams and increases at the lower part due to drainage. In addition to this, the height of the foam is reduced. Shrinkage starts at the bottom of the sample after 150 s, visible in Fig. 4f as the sample recedes from the bottom holder and the side heaters.

SUMMARY

A new experimental setup allowed for X-ray radioscopic in-situ observations of the evolution of Alporas-type foams made by refoaming samples previously quenched in the early pore formation stage.

Due to the fast decomposition of TiH_2 the precursors contained a high level of porosity. Images in early pore stages and near maximum expansion revealed that 100 s of mixing time after the addition of TiH_2 provides the best foamable precursors from the series studied. After this long mixing time the precursor expanded to higher values even though less hydrogen is available in this state. It seems as if there are more usable pore nuclei in such a state.

REFERENCES

1. Ashby, M.F. et al. 2000. "Metal Foams, a design guide", Butterworth-Heinemann Ltd., Boston
2. Banhart, J. 2001. "Manufacture, characterisation and application of cellular metals and metal foams" *Prog. Mat. Sci.*, 46: 559-632.
3. Miyoshi, T., M. Itoh, S. Akiyama, and A. Kitahara. 2000. "ALPORAS Aluminium Foam : Production Processes, Properties, and Applications" *Adv. Eng. Mat.*, 4: 179-183.
4. Körner, C., A. Arnold, and R.F. Singer. 2005. "Metal foam stabilization by oxide network particles" *Mat. Sci. Eng. A*, 396: 28-40.
5. Kaptay, G. 2003. "Interfacial criteria for stabilization of liquid foams by solid particles" *Coll. Surf. A*, 230: 67-80.
6. Babcsán, N., Garcia-Moreno, F., and Banhart, J., 2007. "Metal foams-High temperature colloids: Part II: In situ analysis of metal foams", *Coll. Surf. A*, 309: 254-263.
7. Babcsán, N. and J. Banhart. 2006. "Metal foams towards high-temperature colloid chemistry", *Colloidal Particles at Liquid Interfaces*, B.P. Binks and T.S. Horozov eds.: Cambridge University Press pp. 445-499.
8. Wood, J. T. 1998. "Production and Application of Continuously Cast, Foamed Aluminium", in *Metal Foams*, Banhart, J. and Eifert, H. MIT-Verlag, Bremen, pp. 31-35.
9. Leitmeier, D., H. P. Degischer, and H. J. Flankl. 2002. "Development of a Foaming Process for Particulate Reinforced Aluminium Melts", *Adv. Eng. Mat.*, 10:735-740.
10. Akiyama, S., K. Imagawa, A. Kitahara, S. Nagata, K. Morimoto, T. Nishizawa, and M. Itoh. 1987. US Patent 4.713.277.
11. Miyoshi, T., S. Hara, T. Mukai and K. Higasi. 2001. "Development of a Closed Cell Aluminium Alloy Foam with Enhancement of the Compressive Strength", *Mater. Trans.*, 10: 2118-2123.
12. Song, Z., J. Zhu, L. Ma and D. He. 2001. "Evolution of foamed aluminium structure in foaming process", *Mat. Sci. and Eng. A*, 298: 137-143.
13. Ma, L. and Z. Song. 1998. "Cellular structure control of aluminium foaming process of aluminium melt", *Scripta Mater.*, 39: 1523-1528.
14. Kadoi, K., M. Tayama, M. Yoshida, and H. Nakae. 2005. "Influence of Viscosity on Foamability of Aluminium Melts", *Porous Metals and Metal Foaming Technology*, H. Nakajima and N. Kanetake, eds.: Japan Institute of Metals (JIMIC-4) pp. 267-272.
15. Garcia-Moreno, F., N. Babcsan and J. Banhart. 2005. "X-ray radioscopy of liquid metalfoams: influence of heating profile, atmosphere and pressure", *Col. Surf. A*, 263 (2005) 290-294.
16. Garcia-Moreno, F., M. Fromme and J. Banhart. 2004. "Real-time X-ray Radioscopy on Metallic Foams Using a Compact Micro-Focus Source", *Adv. Eng. Mat.*, 6: 416-420.
17. Matijasevic-Lux, B, J. Banhart, S. Fiechter, O. Gorke and N. Wanderka. 2006. "Modification of titanium hydride for improved aluminium foam manufacture", *Acta Mater.*, 54: 1887-1900.